

Analysis of atmospheric CO₂ growth rates at Mauna Loa using CO₂ fluxes derived from an inverse model

By PRABIR K. PATRA^{1*}, SHAMIL MAKSYUTOV¹ and TAKAKIYO NAKAZAWA^{1,2}, ¹*Frontier Research Center for Global Change, Japan Agency for Marine-earth Sciences and Technology Center, Yokohama 236 0001, Japan;* ²*Center for Atmospheric and Oceanic Studies, Graduate School of Science, Tohoku University, Sendai 980-8578, Japan*

(Manuscript received 27 October 2004; in final form 19 April 2005)

ABSTRACT

Carbon dioxide (CO₂) growth rates are estimated for a period 1959–2004 from atmospheric CO₂ measurements at Mauna Loa by the Scripps Institute of Oceanography. Only during a few short periods, 1965–1966, 1972–1973, 1987–1988 and 1997–1998, in the last 45 yr have growth rates of atmospheric CO₂ been of a similar magnitude or higher than that due to the total emission from burning of fossil fuels. Using results from a time-dependent inverse (TDI) model, based on observations of atmospheric CO₂ at 87 stations, we establish that El Niño-induced climate variations in the tropics and large-scale forest fires in the boreal regions are the main causes of anomalous growth rates of atmospheric CO₂. The high growth rate of 2.8 ppm yr⁻¹ in 2002 can be predicted fairly successfully by using the correlations between (1) the peak-to-trough amplitudes in the El Niño Southern Oscillation (ENSO) index and tropical flux anomaly, and (2) anomalies in CO₂ flux and area burned by fire from the boreal regions. We suggest that the large interannual changes in CO₂ growth rates can mostly be explained by natural climate variability. Our analysis also shows that the decadal average growth rate, linked primarily to human activity, has fluctuated around an all-time high value of ~1.5 ppm yr⁻¹ over the past 20 yr. A statistical model analysis is performed to identify the regions which have the maximum influence on the observed growth rate anomaly at Mauna Loa.

1. Introduction

The increase in abundance of atmospheric CO₂ has been of considerable interest, since this gas has played a significant role in various aspects of climate change such as global warming, ozone depletion, feedback to the ecosystem and air–sea gas exchange, and is expected to continue do so in the future (see Albritton et al., 2001, for a review). The secular component in the increase in CO₂ concentration is linked mainly to the increase in loading of CO₂ from industrial sources; but the observed growth rate is only about half of that without taking into account the sink due to uptake by the terrestrial biosphere and ocean. On interannual timescales, however, the anomaly in terrestrial CO₂ flux can be as large as the annual industrial emission (Keeling et al., 1995; Battle et al., 2000). A regional breakdown of the global flux anomaly has been made using a time-dependent inverse model of atmospheric CO₂ (Rayner et al., 1999). The variability or anomaly in CO₂ flux is defined as the deviation from a multiyear average flux (seasonal cycle or annual total). The variability in oceanic flux is about the half of that over the land, and is often

in the opposite phase (Battle et al., 2000; Bousquet et al., 2000); this situation also results in a smaller interannual variability in atmospheric CO₂ concentration.

There have been intense discussions on CO₂ growth rates at Mauna Loa during October 2002–2003 in the media (e.g. CNN News, 2004; Reuters, 2004) and in scientific publications (e.g. Bacastow, 1979; Keeling et al., 1996; Taguchi et al., 2003). We have analysed the variation in CO₂ flux on global and regional scales using a newly developed time-dependent inverse (TDI) model. Early results using this inverse modelling framework are being considered for publication elsewhere and are referred to here as PKP05a (Patra et al., 2005) and PKP05b (Patra et al., 2005). In those papers regional CO₂ flux anomalies have been estimated for several land and ocean regions in the tropics and mid and high latitudes for the period 1988–2001. Here we analyse the variation in CO₂ flux in connection with climatic conditions in the tropics and with biomass burning in boreal regions as two separate entities. The main aim of this study, however, is to understand the observed growth rate in atmospheric CO₂ at Mauna Loa, a background monitoring station. We have analysed quantitatively the cause for interannual variability in CO₂ growth rate using TDI model fluxes from the global tropics and boreal lands. Finally, we have shown that based on the relations

*Corresponding author.
e-mail: prabir@jamstec.go.jp

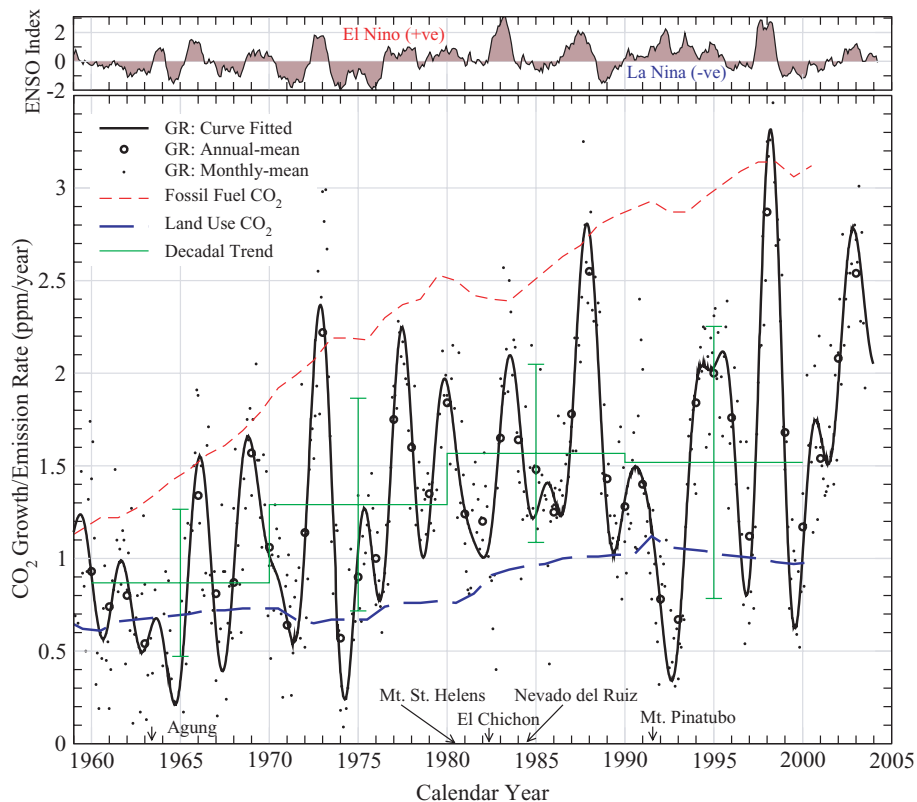


Fig 1. Observed monthly mean (small symbols) and annual mean (large symbols) growth rates in atmospheric CO₂ concentration at the Mauna Loa site (lower panel). The growth rates (GR) are shown as the difference between the monthly mean concentrations between two adjacent years, such that the growth rate for 1 July 1999 is the difference between the CO₂ concentrations in January 2000 and January 1999. This procedure is adopted to study the changes in emission in the current year in comparison with the previous year. The monthly mean growth rates estimated using a fitted curve by digital filtering technique (solid line) are also shown. The growth rates averaged over different decades are shown (thin solid line) and the corresponding spread (1σ) is given as the error bars. The CO₂ emission time-series due to fossil fuel consumption (short-dashed line) (Marland et al., 2003) and land use changes (long-dashed line) (Houghton, 2003) are also shown. The emission rates in Pg of carbon are converted to CO₂ growth rate in ppm with a conversion factor of 2.12 Pg ppm^{-1} (Keeling et al., 2001). The multivariate ENSO index is shown in the top panel. The positive (negative) ENSO phase corresponds to an El Niño (La Niña) period. The times of major volcanic eruptions are given along the bottom axis.

between the TDI flux anomaly and the intensity of El Niño and the estimated area burned by fire, the growth rate of atmospheric CO₂ at Mauna Loa can be predicted a few months in advance.

2. Materials and methods

The direct measurement of atmospheric CO₂ was started in 1958 by C. D. Keeling and co-workers at Mauna Loa, Hawaii (19.5°N , 155.6°W , 3397 m above sea level) (e.g. Keeling et al., 2001). The observations from this station fairly represent the global variability in CO₂, as it is located away from the large continental land masses and at a height above the planetary boundary layer. The monthly and annual averages of observed CO₂ concentrations are used in the analysis. The monthly mean CO₂ concentrations are also fitted by a digital filter to derive the seasonal cycle, the irregular part within the seasonal cycle (also referred to as residuals) and the slowly varying long-term-trend component in the data. We used the filtering method developed by Nakazawa et al. (1997). The Butterworth filter is set to order 26 for long-

term trends and 16 for the seasonal cycle. The trends values are retrieved every month and the growth rates are calculated from the differences in values between successive months. The results from this analysis are depicted in Fig. 1.

The CO₂ flux anomalies derived by the TDI model are used to study the contribution of different source regions to the observed growth rates in atmospheric CO₂ at the Mauna Loa Observatory (MLO). The TDI model is designed to estimate fluxes from 64 partitions of the globe using atmospheric CO₂ data from 87 stations worldwide. The processed data for monthly mean atmospheric CO₂ concentrations are obtained from GlobalView (2002). We have used the NIES/FRCGC tracer transport model (Maksyutov and Inoue, 2000) to simulate the unit (1.0 Pg yr^{-1}) source basis functions for 64 regions and the pre-subtracted sources. Three pre-subtracted flux types are used: annual mean fossil fuel emissions (representing 1990 and 1995), the monthly mean net ecosystem exchange (neutral annual mean) and monthly mean oceanic fluxes. The inverse model framework is Bayesian and the *a priori* fluxes and associated

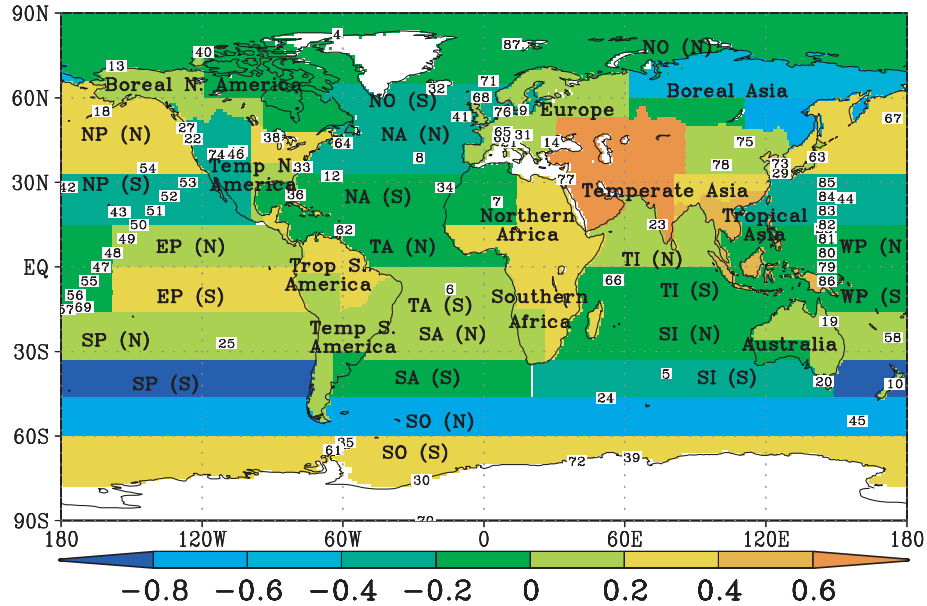


Fig 2. The TDI model regions and CO₂ measurement stations used in this study. The colour bar (shading) indicates the annual mean CO₂ fluxes (in Pg-C yr⁻¹) for the period 1998–2000. Only the TransCom-3 size land regions are labelled; 10 regions have four subdivisions and tropical Asia has two. The abbreviated names are indicated for the oceanic regions as used in this 64-region inverse modelling framework.

uncertainties for each region are based on the weighted mean covariances used in TransCom-3. Further details about this TDI model framework can be found elsewhere (PKP05a). The inverse model regions and observation network used in this study are shown in Fig. 2. Average CO₂ fluxes for the period 1998–2000 are used for shading the TDI model regions. However, to avoid complexity we refrain here from any discussion on regional flux distribution (only flux anomalies are of interest in this study). Here we will focus our discussion mainly on the flux anomalies of two regions: (1) the global tropics, which includes the ocean regions within a latitude belt $\pm 15^\circ$, tropical South America, northern Africa (north of the equator), and tropical Asia (mostly southeast Asia) and (2) boreal Asia and boreal North America (see Fig. 2). We have also aggregated 64-region CO₂ flux anomalies to 22 regions as used in the TransCom-3 studies.

A multiple regression model analysis of CO₂ growth rate ($GR(t)$) has been done for TDI flux anomalies of 22 regions ($f_j(t)$, $j = 1, 22$) to quantify the effect of regional fluxes on GR at MLO. Under this statistical model formulation GR is a linear combination of f_j (a_j are the coefficients):

$$GR(t + L) = a_0 + a_1 f_1(t) + a_2 f_2(t) + \dots + a_{22} f_{22}(t). \quad (1)$$

The regression procedure minimizes χ^2 of the following form (errors in the regional flux anomaly are ignored to give equal weight to all f_j):

$$\chi^2 = \sum_{i=1}^N \left(GR_i - \sum_{j=1}^{22} a_j f_j(i) \right)^2 \quad (2)$$

where N is the length of the time-series, i.e. 52 for 3-month moving window averages in the period April 1988 to March 2001. Time lags (L) have been introduced in the MLO growth rate to estimate the optimal fitting, assuming that the response of growth rate due to the regional flux anomaly will be captured at MLO only after a certain time. This time lag can be understood as the time taken by source signals to reach MLO through atmospheric transport. This analysis is performed using commercially available SAS/STAT software. This program returns values of a_j corresponding to each region's fluxes and F values. The latter indicates the relative significance of regional flux variability in explaining the growth rate.

3. Results and discussion

Figure 1 shows the CO₂ growth rate observed at the MLO (Keeling et al., 2001), along with the emissions due to burning of fossil fuel (Marland et al., 2003), change in land use (Houghton, 2003) and El Niño Southern Oscillation (ENSO) variability in the period 1959–2002. The anomalously high (low) growth rates in atmospheric CO₂ concentration have clearly occurred during the positive (negative) ENSO phases. Only on four occasions (i.e. 1965–1966, 1972–1973, 1987–1988, and 1997–1998) were the CO₂ growth rates observed to be similar in magnitude or higher (Fig. 1, solid line) than that which would be expected from fossil fuel emissions (Fig. 1, short-dashed line), assuming no sinks in the ocean and land biosphere. When the CO₂ growth rates are calculated from monthly mean observations (Fig. 1, small symbols), high values were observed more frequently in 1960, 1969 and 1983–1984 (in addition to the four previously mentioned periods of high growth rate). The TDI model-derived

CO₂ flux anomalies corresponding to total tropics and two boreal land regions are shown in Fig. 3 for the period 1988–2001.

3.1. Effect of ENSO on CO₂ growth rate

The CO₂ flux anomalies from tropical regions are in fairly good agreement with the ENSO variability and positive CO₂ growth rates. Apparently the magnitudes of rates of increase or decrease also correspond well to the amplitude of ENSO variability. For example the 1972–1973 and 1997–1998 El Niño periods were sharply followed and preceded, respectively, by La Niña periods, thus producing the largest increase and decrease in CO₂ growth rate during and after the El Niño periods. This is mainly due to the response of the tropical ecosystem to climate variation. During the El Niño years, under less efficient photosynthesis in the water-stressed regions and increased heterotrophic respiration, the soil tends to gain nutrients; upon the arrival of La Niña the tropical land then becomes more productive. On the contrary, when an El Niño event occurs following a La Niña period, larger

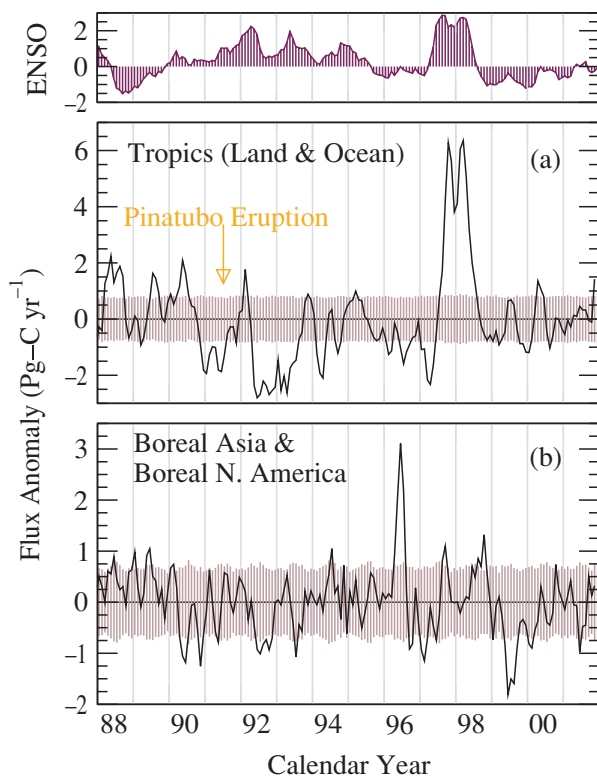


Fig. 3. Estimated CO₂ flux anomaly for (a) total tropics (land + ocean) and (b) boreal regions in Asia and North America. The 3-month running mean is taken for the flux anomaly to reduce the noise. The ENSO index is plotted in the top panel for reference. The TDI model estimated *a posteriori* flux uncertainties are shown as vertical bars along the zero flux. However, we believe the uncertainty in flux anomaly is smaller than those estimated for the TDI fluxes. Note that the CO₂ flux anomaly for the tropical belt crosses the error bars more frequently than for the boreal regions.

than average biomass is available near the ground that can dry and burn under conditions of below normal rainfall and hotter air temperature in the tropics. This hypothesis is supported by region-specific studies for Arizona and New Mexico (Swetnam and Betancourt, 1990). Note that a greater area burns during La Niña years (dry winters) than during El Niño years (wet winters) in the southwest United States, which occur in opposite phase from the tropics. The pattern is that wet El Niño years creating a build-up of fine fuels (grasses and shrubs) which then dry out and ignite more effectively during the dry and warm La Niña years. This process is confirmed by an analysis of individual fire histories at many sites throughout the southwest United States (<http://www.ispe.arizona.edu/climas/>). The responses of the terrestrial ecosystem in relation to a wetter and cooler, or drier and warmer, climate are broadly similar in most environments, but the intensity of the response varies between tropics, mid-latitudes and polar regions.

3.2. CO₂ growth rate and volcanic eruptions

The major volcanic eruptions appeared to have globally dampened the effect of El Niño on increase in atmospheric CO₂ for the periods 1983–1984 (El Chichon) and 1991–93 (Mount Pinatubo) (see Figs 1 and 3). Recent studies have suggested that in the years after a major volcanic eruption (i.e. when there is an abundance of sulphate aerosols in the atmosphere), heterotrophic respiration decreases due to a lowering of the Earth's surface temperature (Lucht et al., 2002) or the productivity of ecosystems in forested area increases under enhanced diffuse radiation (Gu et al., 2003). Both processes lead to a negative anomaly in CO₂ growth rate. A reduction in CO₂ flux (negative anomaly) from the tropical region is also estimated to have occurred during 1991–1993, following the eruption of Mount Pinatubo in June 2001 (Fig. 3). Using the fit between the trends in the ENSO index and CO₂ flux anomaly (Fig. 4a, dashed line), we estimate a collective reduction in 1991 in the trend of the CO₂ flux anomaly from the tropical land regions of up to about 1.8 Pg-C yr⁻¹. The reduction is caused by both suppression of the 1991–1992 El Niño effect on land emissions and processes associated with increased amounts of aerosol in the atmosphere. However, the periods of largest drop (crest to trough) in observed MLO growth rates are found during the La Niña years in 1973–1974, 1988–1989 and 1998–1999 (Fig. 1).

3.3. Changes in interdecadal growth rates

From the spreads in decadal averages, we find that the 1990s was most eventful decade since the start of direct measurements of CO₂. Whether this suggests that the carbon cycle system is becoming vulnerable to climate variations can be debated. However, the stabilizing trend in CO₂ emission from change in land use and land management may be noted (Houghton, 2003). Some studies have also indicated that vegetation greening due to an

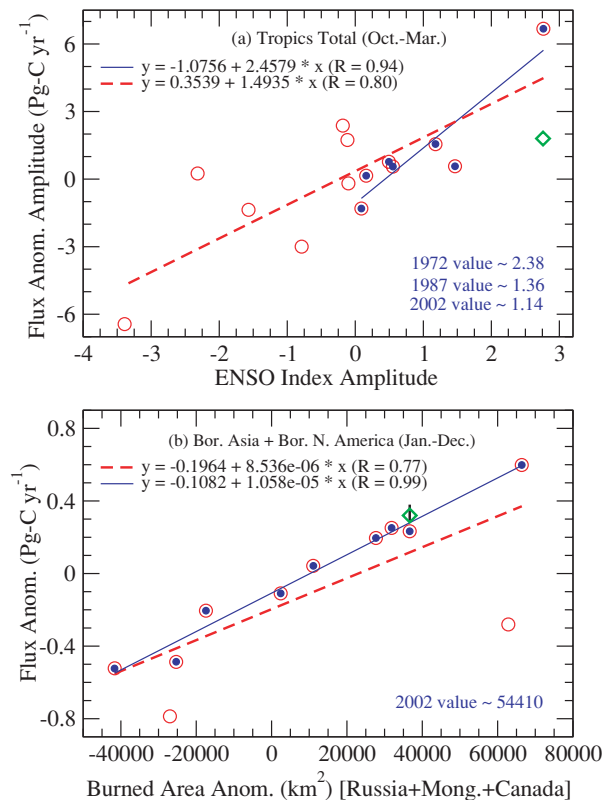


Fig 4. Correlations of (a) amplitudes between adjacent peaks and troughs (also referred to here as gradients) in annual mean CO₂ flux anomaly for the tropical belt with ENSO index trends (October–March averages) and (b) anomalies in CO₂ flux and burned area in boreal regions (Canada, Mongolia and Russia) (January–December averages). The fire statistics are taken from Stocks et al. (2003) for Canada and Forest Resource Assessment (2001) for Mongolia and Russia. The *x*-axis values for several distinct years, not covered in TDI model simulations or in the fittings, are given within each panel. These numbers are used for testing the predictive value of both the fitted curves. For panel (a) the trends are calculated by subtracting the values for the previous year from the current year (all positive/negative/neutral ENSO years are considered for the fit, dashed line). The fit using the positive ENSO years only (solid line and solid symbols) is also shown for comparison. For boreal regions (b) two separate data selections are also used in the linear fits (the one with all data is used for discussion). Some other estimations of carbon emission due to fires only are shown for comparison: in panel (a) for tropical South America and southeast Asia and in panel (b) for the northern boreal regions (diamonds) (van der Werf et al., 2004) and for boreal Asia and North America (vertical bar in b) (Kasischke and Bruhwiler, 2003).

increase in the Earth's surface temperature in the mid- and high latitudes, increase in solar radiation in the tropics and higher CO₂ concentration in the atmosphere has led to increased net primary production by the land ecosystem (e.g. Nemani et al., 2003). The results of our TDI model for the period 1988–2001 suggest an increase in the Northern Hemisphere land sink (~ 0.5 Pg-C yr⁻¹), a stable Southern Hemisphere flux and an increase of about 1.5 Pg-C yr⁻¹ in the tropical land source (see PKP05b). The

values given here represent average budgets for the respective regions during 1988–2001. The large increase in the tropical land source is biased by the enhanced carbon sink following the eruption of Mount Pinatubo in the early 1990s and the enhanced carbon source due to the 1997–1998 El Niño event. On the other hand, stratification and heating of the upper ocean in the past decades have produced a tendency towards a larger oceanic sink (Keeling and Garcia, 2002). We believe that these processes have jointly helped to stabilize the decadal average CO₂ growth rates in the last two decades, despite the increase in emission from combustion of fossil fuels. However, the present CO₂ growth rate (~ 1.5 ppm yr⁻¹) is the fastest ever since records of atmospheric CO₂ concentration began (Barnola et al., 1987), and the growth rate was only about 0.9 ppm yr⁻¹ in the 1960s (Fig. 1).

3.4. Tropical flux anomalies and the CO₂ growth rate

The land areas of the tropics are most susceptible to the changes in meteorological conditions due to the ENSO. During the El Niño periods, low relative humidity/rainfall and high average air temperature apparently lead to more forest fires and reduced ecosystem production (i.e. drought-like conditions). A recent study based on inverse modelling of atmospheric CO₂ and biogeochemical modelling quantitatively illustrated the link between El Niño and enhanced release of carbon from different biospheres (PKP05b). Here we have used the CO₂ fluxes from the tropical latitude belt (both land and ocean regions, see Fig. 3a) for the period 1988–2001 and the ENSO index to quantify the role of El Niño on the CO₂ flux anomaly (Fig. 4a). Because the response of tropical land and ocean CO₂ fluxes to the ENSO are generally anticorrelated and only the net surface flux controls the growth rate, we have treated the CO₂ fluxes from the tropical land and ocean in combination. The estimated CO₂ emission due to fires in the 1997–1998 El Niño period (van der Werf et al., 2004) generally underestimates the trends in the CO₂ flux anomalies derived from the TDI model. This is because responses of ecosystems to climate variability constitute a large fraction of the CO₂ flux anomaly for the tropical land biosphere (PKP05b).

A compact relation between the gradients in the ENSO index and the CO₂ flux anomaly is apparent (Fig. 4, dotted line, correlation coefficient $R = 0.80$). The correlation increases further ($R = 0.94$) if only the El Niño events are considered. These correlations are significant at a 99% confidence level. However, the fit using all the data will be used in the following discussions. Based on the correlation and trend of the ENSO index, we estimate a net CO₂ flux anomaly of about +4.0 Pg-C yr⁻¹ from the tropics during 1972–1973, which is sufficient to explain the observed increase (trough to crest) in CO₂ growth rate of about 1.8 ppm yr⁻¹. For the 1987–1988 case (increase in growth rate of about 1.4 ppm yr⁻¹) a flux anomaly of about +2.35 Pg-C yr⁻¹ is estimated from the tropics. Of the remaining, about 0.5 Pg-C yr⁻¹ was supplied by the severe forest fires in northern China and

eastern Siberia during May–June 1987 (Cahoon et al., 1994). Generally the forest fires provide a large fraction of the total CO₂ emission in different climatic zones, as seen in Fig. 4. The difference between CO₂ emissions estimated from forest fire statistics (diamonds) and TDI estimates (circles) arises from the response of the ecosystem to the meteorological conditions. The prediction of the CO₂ flux anomaly for 2002–2003 is about +2.1 Pg-C yr⁻¹ from the tropics, which can increase the growth rate by about 1.0 ppm yr⁻¹ globally. This is less than that required (approximately 0.3 ppm yr⁻¹ from the low value of 1.5 ppm yr⁻¹ at the trough) to attain a growth rate of 2.8 ppm yr⁻¹ in 2002 (see Fig. 1).

3.5. Effect of boreal fires on CO₂ growth rate

Here we look for other sources of anomalous CO₂ emission in the form of boreal forest fires. The CO₂ flux anomaly arising from tropical forest fires is included in Fig. 4a. Forest fire statistics from several countries are available in the Global Forest Fire Assessment Report (Forest Resource Assessment, 2001). According to that the total burned area or fire counts are observed to be the highest in the Russian Federation, Canada and Mongolia. The satellite maps indicate a rise in fire activity in Russia during 1998 to 2003, with the largest ever occurrence of fire in 2003 (Sukhinin et al., 2003). The fire statistics for Canada are taken from Stocks et al. (2003). Since the occurrence of forest fires in boreal regions does not follow any specific climate variability (PKP05b), we have plotted the burned area anomaly versus CO₂ flux anomaly as derived from inverse model (Fig. 4b). Annual mean CO₂ flux anomalies are constructed using the values in Fig. 3b. A comparison with other independent estimations (Kasischke and Bruhwiler, 2003; van der Werf et al., 2004) of CO₂ emission due to boreal forest fires shows good agreement with our results. This suggests that the differences in ecosystem production (respiration) due to climate variability not accounted for here only occasionally play a significant role in the boreal region or are in the opposite (same) phase to the occurrence of fire. However, two large deviations from the fitted line are probably caused by the responses of the ecosystem to the regional climate (e.g. -0.79 or 0.28 Pg-C yr⁻¹ flux anomaly values corresponding to -26 500 or 62 800 km² burned area anomaly, respectively, during 1999 and 1997). We find a fit between the TDI model flux anomaly and the burned area anomaly for the boreal regions (Canada, Mongolia, and Russia) in the period 1989–1999 ($R = 0.77$, significant at a 99% confidence level). If we omit two outliers for the fitting, a better correlations is obtained ($R = 0.99$). Though Mongolia is not included in the boreal Asia region of our inverse model, we have added its burned area anomaly to that of Canada and Russia in this correlation exercise. Since the Mongolian fires are dominant in the boreal summer season, when the trade winds are typically southwesterly, we believe that the CO₂ emission signal is not captured at the Ulaan Uul site, located near the southern border of Mongolia. Thus the CO₂ flux

due to Mongolian biomass burning is likely to be misallocated to the regions in boreal Asia.

We find about a difference of about a factor of 2 in the fire area/fire counts from estimates based on forestry inventory and satellite imagery for the overlapping period of 1996–1999 Forest Resource Assessment (2001), Sukhinin et al. (2003). Thus there was difficulty in extrapolating our fit between the burned area anomaly using the Forest Resource Assessment (2001) burned area database and the CO₂ flux anomaly (Fig. 4b) for the 2002 burned area estimations of 117 700 km² using satellite data (Sukhinin et al., 2003). Therefore, we have taken a separate long-term average ($\approx 73\,800$ km²) for the Sukhinin et al. (2003) data set for the period 1996–2002. Thus a burned area anomaly of 43 900 km² (4.39×10^6 ha) is calculated from Russia alone during 2002. The burned area statistics for Canada are available from the Natural Resources Canada report (<http://www.nrcan-rncan.gc.ca/inter/index.html>). We estimate an burned area anomaly of 10 500 km² for 2002 with respect to an average for the period 1996–2002 of $\approx 17\,500$ km² for Canada. From the best fit (using all data) between CO₂ flux anomaly and boreal fires (Fig. 4b, dashed line), we estimate a CO₂ flux anomaly of about 0.28 Pg-C yr⁻¹ in 2002, assuming the burned area anomaly for Mongolia to be small in 2002. This flux can increase the CO₂ growth rate by about 0.13 ppm yr⁻¹ globally. However, since the boreal North America and boreal Asia region are closely connected by atmospheric dynamics to MLO, a larger impact on the MLO-observed increase in growth rate is expected. If the flux anomaly is confined to the Northern Hemisphere it would increase the CO₂ concentration at the MLO by about 0.26 ppm yr⁻¹. This estimation is about equal to the growth rate (~ 0.3 ppm yr⁻¹), in addition to the tropical flux anomaly, necessary to explain the anomalous MLO growth rate in 2002.

3.6. Statistical analysis of CO₂ TDI fluxes and MLO growth rate anomalies

Finally, we have performed multiple regression analysis of the CO₂ growth rate anomaly at MLO and TDI modelled flux anomalies from 22 TransCom-3 regions. Regression analysis examines the relationship between a response (i.e. growth rate anomaly) and a set of explanatory variables (i.e. regional flux anomalies). The results are shown in Fig. 5 and Table 1. It is clear from Fig. 5 that the TDI flux anomalies without any time lag do not explain in detail features present in the variability of CO₂ growth rate at MLO. The analyses using different time lags between CO₂ regional fluxes and observed growth rates suggest that a lag of about 9 months produces the best match between observations and regression model results (not shown). A rather long time lag also indicates that the Northern Hemisphere tropics alone do not control all the variability in CO₂ growth rate recorded at MLO. Larger F values in Table 1 suggest a greater similarity between the time-series of MLO-observed growth rate and

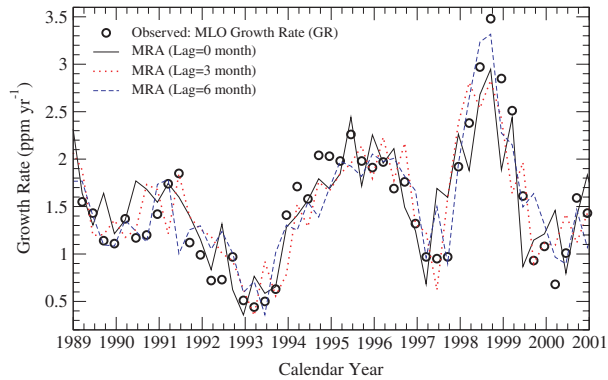


Fig 5. Growth rate anomaly observed at MLO (symbols) and those obtained from a multiple regression analysis (MRA, eq. 1) of TDI CO₂ flux anomaly for 22 TransCom-3 regions. The line types correspond to a set of regional flux coefficients (a_j , see Table 1) when 0, 3 and 6 months time lags in the observed CO₂ growth rate anomaly are introduced. The χ^2 for each of these cases are 6.68 ($L = 0$, solid line), 5.88 ($L = 3$, dotted line) and 4.53 ($L = 6$, dashed line), respectively.

regional CO₂ fluxes. When the flux anomalies are in opposite phase to the growth rates a negative a value is estimated (e.g. tropical East Pacific), and vice versa. The regions associated with larger a values do not necessarily mean a stronger influence on the MLO-observed growth rate. For example, because the flux variability of tropical Asia is large and is in phase with the MLO-observed growth rate a smaller a value can explain a significant part of the growth rate (i.e. large F).

Tracer transport is apparently efficient (transport time ~ 2 –3 months) from tropical and boreal Asia, the North Pacific and tropical Atlantic to the MLO, and CO₂ flux anomalies are in phase with CO₂ growth rates (Table 1, $L = 3$). Since the source signal from tropical South America does not reach the MLO directly during August to November, the period of high CO₂ flux anomaly, very high F values are not estimated. At $L = 6$, the regional CO₂ fluxes that contribute to the MLO growth rate anomaly are mostly of hemispheric to global scale and are slow varying. This is apparent from the smaller a values (less than 1.0) associated with all regions. This result also indicates the greater

Table 1. Coefficients a_j (eq. 1) and F values as estimated by the regression analysis for different lag times (L) in CO₂ growth rate. The regions associated with values greater than 1.5 or so apparently have a similar flux variability to the MLO growth rate, i.e. those regions make a significant contribution to construction of the regression fits. Using Pearson's correlation analysis we find that 69, 72, 77, 81 and 77% of the growth rate variability can be explained by TDI CO₂ fluxes with lag times of 0, 3, 6, 9 and 12 months, respectively.

Flux region	a values for different L			F values for different L		
	$L = 0$	$L = 3$	$L = 6$	$L = 0$	$L = 3$	$L = 6$
Boreal North America	2.17	0.14	0.14	0.10	0.00	0.81
Temperate North America	1.22	0.02	-0.07	0.11	0.00	0.90
Tropical South America	2.17	0.14	0.14	0.27	1.16	1.52
Temperate South America	1.22	0.02	-0.07	0.00	0.00	0.14
North Africa	-0.75	-0.29	0.04	13.39	2.22	0.06
South Africa	0.06	0.10	0.01	0.09	0.32	0.00
Boreal Asia	0.21	0.23	0.06	2.55	3.76	0.34
Temperate Asia	0.29	0.18	0.25	4.40	1.97	3.59
Tropical Asia	0.75	0.73	0.45	12.45	13.42	6.29
Australia	0.75	0.49	0.61	3.83	1.75	3.20
Europe	-0.42	-0.27	-0.22	4.55	2.11	1.75
North Pacific	0.68	0.53	0.28	7.07	4.71	1.59
Tropical West Pacific	0.03	0.19	-0.10	0.00	0.29	0.09
Tropical East Pacific	-0.34	-0.26	-0.65	0.54	0.35	2.70
South Pacific	0.17	0.06	0.49	0.41	0.05	4.75
Northern Ocean	1.17	0.33	-0.15	2.25	0.20	0.05
North Atlantic	-0.66	-0.31	-0.45	1.51	0.38	1.01
Tropical Atlantic	2.34	1.58	0.67	11.88	6.22	1.36
South Atlantic	0.43	0.50	0.21	0.58	0.92	0.18
Southern Ocean	-0.06	-0.15	0.10	0.03	0.23	0.11
Tropical Indian Ocean	-0.06	0.05	0.35	0.08	0.06	3.36
South Indian Ocean	0.32	0.38	0.46	0.52	0.88	1.53

spatial representativeness of the MLO station for observations of atmospheric CO₂.

Our results may imply that it is possible to construct a model to predict CO₂ flux (or growth rate) for the tropical and northern boreal regions, each region, respectively, requiring information on the ENSO index and fire statistics (area burned) mainly from Canada, Mongolia and Russia. However, the validity of such a predictive system depends on the present level of human and natural influences on the land biosphere, such as changes in land use and land use management, agricultural practices and forest fire management.

4. Conclusions

We have used the CO₂ measurements from Mauna Loa to calculate the atmospheric growth rates for the period 1958–2002. The CO₂ flux anomalies (1988–2001) from the tropical land and ocean and from boreal Asia and boreal North America estimated using the inverse model have been used to produce compact relationships with the trend of the ENSO index and burned area anomaly, respectively. These relations are used to predict the CO₂ flux anomalies for the periods 1972–1973, 1987–1988 and 2002–2003. The predicted flux anomalies can explain fairly well the observed high CO₂ growth rates in those periods. Our analysis suggests that the CO₂ flux anomaly due to activity of the biosphere (photosynthesis and respiration) and biomass burning responds in phase with the climate variability (e.g. ENSO) in the tropical biosphere. But CO₂ fluxes from the boreal ecosystem are under the greater influence of biomass burning. The decadal average growth rate appears to have stabilized in the last two decades at a very high level (~1.5 ppm yr⁻¹), compared with a 0.9 ppm yr⁻¹ rate in the 1960s. While the high growth rate is caused by the increase in fossil fuel consumption and changes in land use management, the stabilization is attributed to enhanced uptakes of CO₂ by the land and ocean over the same period of time. The statistical regression model analysis helps us to quantify the contribution of TDI model simulated regional fluxes on the observed CO₂ growth rates at MLO, and identify the flux regions having maximum impact. We believe that the analysis performed in this study also indicates the overall validity of the CO₂ flux anomalies derived using the 64-region TDI model and the NIES/FRSGC global transport model framework.

5. Acknowledgments

We thank C. D. Keeling and co-workers at SIO for making their observational data available freely; without that this work would not be feasible. P.K.P. is grateful to Xiaoyuan Yan for running multiple regression analysis on the MLO GR and TDI flux datasets using SAS/STAT software. We thank both the reviewers (Pieter Tans and anonymous) for critical comments and thoughtful suggestions which have much improved this manuscript.

References

- Albritton, D. L., Allen, M. R., Baede, A. P. M., Church, J. A., Cubasch, U. and co-authors 2001. Summary for policymakers. In: *Climate Change 2001: The Scientific Basis* (eds J. T. Houghton, Y. Ding, D. Griggs, M. Noguer, P. van der Linden, D. and co-editors). Cambridge University Press, Cambridge, 1–83.
- Bacastow, R. B. 1979. Dip in the atmospheric CO₂ level during the mid-1960's. *J. Geophys. Res.* **80**, 3109–3114.
- Barnola, J.-M., Raynaud, D., Korotkevich, Y. S. and Lorius C. 1987. Vostok ice core provides 160,000-year record of atmospheric CO₂. *Nature* **329**, 408–14.
- Battle, M., Bender, M. L., Tans, P. P., White, J. W. C., Ellis, J. T. and co-authors 2000. Global carbon sinks and their variability inferred from atmospheric O₂ and δ¹³C. *Science* **287**, 2467–2470.
- Bousquet, P., Peylin, P., Ciais, P., Quéré, C. L., Friedlingstein, P. and co-author 2000. Regional changes in carbon dioxide fluxes of land and ocean since 1980. *Science* **290**, 1342–1346.
- Cahoon, D. R., Stocks, B. J., Levine, J. S., Cofer, W. R. III and Pierson, J. M. 1994. Satellite analysis of the severe 1987 forest fires in northern China and southeastern Siberia. *J. Geophys. Res.* **99**, 18 627–18 638.
- CNN News, 2004. Carbon dioxide buildup accelerating, 20 March 2004, (www.cnn.com).
- Forest Resource Assessment (FRA). 2001. *Global Forest Fire Assessment 1990–2000*. FAO Working Paper 55. Food and Agriculture Organisation of the United Nations, Rome.
- GLOBALVIEW-CO₂. 2002. *Cooperative Atmospheric Data Integration Project—Carbon Dioxide*. CD-ROM. NOAA CMDL, Boulder, CO. (Anonymous FTP to <ftp://ftp.cmdl.noaa.gov/ccg/co2/> GLOBALVIEW/)
- Gu, L., Baldocchi, D. D., Wofsy, S. C., Munger, J. W., Michalsky, J. J. and co-authors 2003. Response of a deciduous forest to the Mount Pinatubo eruption: enhanced photosynthesis. *Science* **299**, 2035–2038.
- Houghton, R. A. 2003. Revised estimates of the annual net flux of carbon to the atmosphere from changes in land use and land management 1850–2000. *Tellus* **55B**, 378–390.
- Kasischke, E. S. and Bruhwiler, L. P. 2003. Emissions of carbon dioxide, carbon monoxide, and methane from boreal forest fires in 1998. *J. Geophys. Res.* **108**, doi:10.1029/2001JD000461.
- Keeling, C. D., Chin, J. F. S. and Whorf, T. P. 1996. Increased activity of northern vegetation inferred from atmospheric CO₂ measurements. *Nature* **382**, 146–149.
- Keeling, R. F. and Garcia, H. E. 2002. The change in oceanic O₂ inventory associated with recent global warming. *Proc. Natl. Acad. Sci. USA* **99**, 7848–7853.
- Keeling, C. D., Whorf, T. P., Wahlen, M. and van der Plicht, J. 1995. Interannual extremes in the rate of rise of atmospheric carbon dioxide since 1980. *Nature* **375**, 666–670.
- Keeling, C. D., Whorf, T. P., Wahlen, M. and van der Plicht, J. 2001. Exchanges of atmospheric CO₂, and ¹³CO₂, with the terrestrial biosphere and oceans from 1978 to 2000. *SIO Reference Series no. 00–21*, Scripps Institution of Oceanography, University of California, San Diego, CA.
- Lucht, W., Prentice, I. C., Myneni, R. B., Sitch, S., Friedlingstein, P. and co-authors 2002. Climatic control of the high-latitude vegetation greening trend and the Pinatubo effect. *Science* **296**, 1687–1689.

- Maksyutov, S. and Inoue, G. 2000. Vertical profiles of radon and CO₂ simulated by the Global Atmospheric Transport Model. In: *CGER Supercomputer Activity Report* CGER/NIES-I039-2000, (7), 39–41.
- Marland, G., Boden, T. A. and Andres, R. J. 2003. Global, regional, and national fossil fuel CO₂ emissions. In: *Trends: a Compendium of Data on Global Change*. CDIAC, Oak Ridge National Laboratory, Oak Ridge, TN. <http://cdiac.esd.ornl.gov>
- Nakazawa, T., Ishizawa, M., Higuchi, K. and Trivett, N. B. A. 1997. Two curvefitting methods applied to CO₂ flask data. *Environmetrics* **8**, 197–218.
- Nemani, R. R., Keeling, C. D., Hashimoto, H., Jolly, W. M., Piper, S. C. and co-authors 2003. Climate-driven increases in global terrestrial net primary production from 1982 to 1999. *Science* **300**, 1560–1563.
- Patra, P. K., Maksyutov, S., Ishizawa, M., Nakazawa, T., Takahashi, T. and Ukita, J. 2005a. Interannual and decadal changes in the sea-air CO₂ flux from atmospheric CO₂ inverse modelling. *Global Biogeochem. Cycles*, provisionally accepted, doi: 10.1029/2004GB002257.
- Patra, P. K., Ishizawa, M., Maksyutov, S., Nakazawa, T. and Inoue, G. 2005b. Role of biomass burning and climate anomalies for land-atmosphere carbon fluxes based on inverse modelling of atmospheric CO₂. *Global Biogeochem. Cycles* **19**, GB3005, doi: 10.1029/2004GB002258.
- Rayner, P. J., Enting, I. G., Francey, R. J. and Langenfelds, R. 1999. Reconstructing the recent carbon cycle from atmospheric CO₂, δ¹³C and O₂/N₂ observations. *Tellus* **51B**, 213–232.
- Reuters, 2004. Greenhouse gas jump spurs global warming fears, 11 October 2004, (www.reuters.com).
- Stocks, B. J., Mason, J. A., Todd, J. B., Bosch, E. M., Wotton, B. M. and co-authors 2003. Large forest fires in Canada, 1959–1997. *J. Geophys. Res.* **108**(D1), doi:10.1029/2001JD000484.
- Swetnam, T. W. and Betancourt, J. L. 1990. Fire–Southern Oscillation relations in the southwestern United States. *Science* **249**, 1017–1020.
- Sukhinin, A., Ivanov, V. V., Ponomarev, R. I., Slinkina, O. A., Cherepanov, A. V. and co-authors 2003. The 2002 fire season in the Asian part of the Russian Federation: a view from space. *Int. Forest Fire News*, No. 28, Part III, 18–28.
- Taguchi, S., Murayama, S. and Higuchi, K. 2003. Sensitivity of interannual variation of CO₂ seasonal cycle at Mauna Loa to atmospheric transport. *Tellus* **55B**, 547–554.
- van der Werf, G. R., Randerson, J. T., Collatz, G. J., Giglio, L., Kasibhatla, P. S. and co-authors 2004. Continental-scale partitioning of fire emissions during the 1997 to 2001 El Niño/La Niña period. *Science* **303**, 73–76.